High-resolution visible spectrum for the $A^3\Pi(1)-X^1\Sigma^+$ system of IBr

DOMINIQUE R.T. APPADOO, PETER F. BERNATH,[1] AND ROBERT J. LE ROY[1]
Guelph–Waterloo Centre for Graduate Work in Chemistry, University of Waterloo, Waterloo, ON N2L 3G1, Canada

Received April 4, 1994
Accepted July 5, 1994

This paper is dedicated to Dr. Gerhard Herzberg on the occasion of his 90th birthday

New high-resolution absorption and laser excitation spectra of the $A^3\Pi(1)-X^1\Sigma^+$ system of IBr, consisting of approximately 4000 lines of over 40 bands spanning the vibrational range $v' = 6-29$ and $v'' = 1-4$ for each of the two isotopomers, have been recorded and analyzed. Combined with previous microwave and infrared data and fluorescence progressions into the X state, and with new data obtained from laser excitation of the lowest levels of the A state, they formed the core of a global fit to mass-reduced Dunham expansions that yields new molecular constants for the A and X states of $I^{79}Br$ and $I^{81}Br$. Inability to fully account for all data within the experimental uncertainties points to the existence of substantial perturbations or "non-mechanical" behaviour for A-state levels $v' > 24$.

Le spectre du système the $A^3\Pi(1)-X^1\Sigma^+$ de la molécule de bromure d'iode enregistré par absorption à haute résolution et par excitation laser a été analysé. Pour chaque espèce isotopique, quelques 4000 transitions ont été mesurées; celles-ci forment plus de 40 bandes provenant des niveaux vibrationels $v' = 6-29$ de l'état électronique excité A et $v'' = 1-4$ de l'état fondamental X. Des raies microondes, infrarouges et de fluorescence dans l'état X, aussi bien que de nouvelles informations obtenues par excitation laser de l'état A ont été ajoutées aux nouvelles transitions rovibroniques de cette étude; celles-ci forment la base d'une régression linéaire globale. Les transitions appartenant aux deux espèces isotopiques ont permis d'ajuster les paramètres des expansions à masses réduites de Dunham. Les valeurs des constantes spectroscopiques représentant les états électroniques X et A des molécules $I^{79}Br$ et $I^{81}Br$ ont ainsi été améliorées. L'incapabilité de reproduire les raies observées, à l'intérieur des incertitudes expérimentales, démontre l'existence de perturbations ou de comportements « non-méchaniques » importants dans la region des niveaux vibrationels $v' > 24$ de l'état A.

Can. J. Phys. **72**, 1265 (1994)

1. Introduction

Diatomic halogens are among the most widely studied molecules in chemistry. However, there are considerable differences in the quality and quantity of the spectroscopic data available for each species. In particular, IBr has been the subject of numerous previous spectroscopic studies, spanning the region from the microwave to the ultraviolet [1–11]. However, the upper state of one of the main visible transitions is still relatively poorly known, and most previously reported sets of constants were based mainly on treatment of a single type of data considered in isolation, so no sound overall description of this system has appeared. To address this problem, the present paper reports extensive new measurements of the visible $A^3\Pi(1)-X^1\Sigma^+$ band system of IBr, and utilizes them in an empirical combined-isotopes Dunham analysis that takes account of as much as possible of the relevant previously measured data.

One of the earliest studies of the $A-X$ system of IBr was Brown's 1932 absorption measurement of band-heads belonging to transitions between $v' = 8-43$ and $v'' = 0-4$ [1]. However, although he accessed higher vibrational levels of the A state than any subsequent study, Brown's data were omitted from the present analysis because of their low resolution and because (see below) the upper vibrational levels of the A state are perturbed. A more comprehensive and higher resolution absorption study of this system was reported in 1962 by Selin [2], who observed rovibronic transitions between $v' = 9-32$ and $v'' = 0-3$. While his work yielded the first realistic overall set of constants for the A state, the very long extrapolation below $v' = 9$ left its electronic energy and conventional low-order spectroscopic constants relatively uncertain. Since the extensive new data reported herein are of higher accuracy and reach lower v' values, Selin's measurements were also omitted from the data set used in the present analysis. Much more recently, Suzuki and Fujiwara used diode laser spectroscopy to observe 37 rovibrational transitions of the $A-X$ system at high resolution [8]. The accuracy of their data is comparable to that of the present measurements, so they are utilized in the present analysis.

In the microwave region, Tiemann and Möller [3] and Willis and Clark [6, 7] observed pure rotational transitions in the X state for both isotopomers of IBr; for $I^{79}Br$ the observed vibrational levels were $v = 0-4$, and for $I^{81}Br$ they were $v = 0-5$. These data are an essential component of the present data set.

In 1993, Campbell and Bernath used Fourier transform spectroscopy to obtain the first high-resolution infrared spectrum of IBr [10]. They observed the 1–0 and 2–1 bands for both isotopomers and reported accurate spectroscopic constants for the X state based on fits to both their measurements and the microwave data of Willis and Clark [6, 7]. Earlier this year, however, their work was superseded by even more accurate and extensive far-infrared vibration–rotation spectra recorded using a synchrotron as the light source for a Fourier transform spectrometer,[2] which extended the vibrational infrared spectrum to include the 3–2 band. Both the microwave data and these new synchrotron-based infrared data are included directly in the present analysis, and largely define the properties of the lower vibrational levels of the X state.

For higher X-state levels, extensive rovibrational information is provided by Weinstock and Preston's laser-induced fluorescence measurement of several series of progressions

[1]Authors to whom correspondence may be addressed.

[2]B. Nelander, V. Sablinskas, V. Braun, M. Dulick, and P. Bernath. Manuscript in preparation.

TABLE 1. Ranges of v' levels observed in the present absorption and laser excitation experiments

	v' range	
v''	$I^{79}Br$	$I^{81}Br$
1	16–25, 27–29	16–29
2	7–16, 25, 27, 28	7–16, 21–25, 27, 28
3	6, 9–13, 19–21	6, 9–13, 19–21
4	10–13	10–13

belonging to the $B'^3\Pi(0^+) \rightarrow X\,^1\Sigma^+$ system [4, 5]. For four B'-state levels of each of $I^{79}Br$ and $I^{81}Br$, they observed P/R doublet emission into a series of X-state vibrational levels spanning the range $v'' = 0$–19. Although of somewhat lower accuracy than the other data used in the present fits, these results provide essential information regarding the higher lying vibrational levels of the ground electronic state.

One further type of information used in the present analysis was obtained from novel experiments reported by Zheng et al. [9] and Clevenger et al. [11]. They used ultraviolet photolysis to prepare A-state IBr in a free jet expansion, and then recorded laser excitation spectra for transitions from the lowest vibrational levels of the $A\,^3\Pi(1)$ state to high vibrational levels of the $\beta(1)$ state, which belongs to the first tier of IBr ion-pair states. This yielded the first direct observation of transitions associated with the lowest vibrational levels of the A state; these data are quite important, since none of the other results for this system provided information on A-state levels below $v = 6$. The exploitation of these data is made complicated by the fact that the $\beta(1)$ state levels associated with these transitions are perturbed by levels of the neighbouring D state. However, Clevenger et al. [11] have reported a careful deperturbation analysis which yielded B_v and $T_{v,0}$ values for the three lowest vibrational levels of the A state, and these quantities were included directly in the present global fits to determine an optimal set of spectroscopic constants for the A–X system.

In the following, we begin by describing the new experimental information on the $A^3\Pi(1)$–$X^1\Sigma^+$ band system of IBr obtained in the present work. The following section then describes the way the present data analysis combines these new data with other available information on the A and X states in order to determine optimal sets of spectroscopic constants for these electronic states.

2. New measurements of the A–X band system of IBr

2.1. Methods

The experimental part of this work has probed the A–X system of IBr at high resolution using both absorption and laser excitation techniques. In the absorption experiment, a White-type cell was coupled to a Bruker IFS 120 HR Fourier transform spectrometer to provide a sufficiently long path length to record the very weak transitions of the A–X system. A tungsten lamp internal to the spectrometer was the source of radiation, a quartz beamsplitter was used, and the detector was a silicon photodiode. The White cell is 1.2 m in length and 7.5 cm in diameter, and contained approximately 6 Torr of commercial grade IBr at room temperature (1 Torr = 133.3 Pa). The mirrors in the cell were adjusted so that a path length of approximately 10 m was obtained. Spectra were recorded between 12 300 and 14 300 cm^{-1} at a resolution of 0.01 cm^{-1}. In the laser excitation experiment, a Ti:sapphire ring laser (Coherent model 899-29) pumped by a 20 W Coherent Inova-200 argon ion laser was used to excite approximately 3–4 Torr of IBr in a 10 cm Pyrex cell at room temperature. Another cell filled with iodine was used for calibration purposes. Both the I_2 and IBr were purified by vacuum sublimation. The total fluorescence from the iodine cell was detected by a photomultiplier tube, while the total fluorescence from the IBr cell was dispersed through a monochromator before detection by another photomultiplier tube. The Ti:sapphire laser was scanned by a PC computer using the AUTOSCAN soft-ware supplied by Coherent, and the fluorescence from both cells was recorded as a function of the laser wavelength. The emitted radiation was recorded using a monochromator as a filter, to optimize the weak signals. The method of selective fluorescence detection of laser excitation spectra improves the signal-to-noise ratio and provides simpler spectra [12].

2.2. The observed spectra

At room temperature, IBr is in equilibrium with I_2 and Br_2, $I_2 + Br_2 \quad 2\,IBr$, with the mole fraction of I_2 and Br_2 being of the order of 5%, since $K_{eq} \approx 400$ [13]. Fortunately, both I_2 and Br_2 have either weak or no transitions in the region of the A–X transition of IBr. In the near-infrared – visible region, the spectrum of IBr is dominated by the A–X and B–X electronic transitions. The A–X system is just slightly overlapped by the stronger B–X system at shorter wavelengths, and its spectrum is very dense. In addition to having considerable overlap between vibrational bands, each with P, Q, and R branches, the spectrum of the A–X electronic transition is further complicated by the fact that the two naturally occurring isotopes of bromine yield $I^{79}Br$ and $I^{81}Br$ in nearly equal abundance.

The absorption spectrum of IBr was recorded from 12 300 to 14 300 cm^{-1}, with approximately 7600 transitions being observed. The peak positions of the best defined lines have an uncertainty of ca. 0.003 cm^{-1}. The lines were measured using a program called PC-DECOMP, written by J. Brault, which fits the peaks to Voigt lineshapes. They were then arranged into series using the interactive colour spectral assignment program "LOOMIS–WOOD," written by C. Jarman. Over 40 bands, involving transitions between $v'' = 1$–4 and $v' = 9$–29, were observed in absorption (see Table 1). The sample spectrum presented in Fig. 1 shows part of the Q branch of the 11–3 band of both isotopomers. the dense nature of this segments is primarily due to the presence of seven or eight overlapping bands, each with their respective P, Q, and R branches.

The laser excitation spectrum was recorded in the interval from 12 300 to 12 700 cm^{-1}, with approximately 260 transitions being recorded. The lines positions were measured using ASPLOT, a program in the AUTOSCAN software package that controls the Ti:sapphire ring laser. The observed transitions belong to the 6–3, 7–2, 8–2, and 9–2 bands, of which only the last has been observed previously. Figure 2 shows part of the 8–2 band of IBr obtained in this way. Not only has the method of selective fluorescence detection yielded a significant increase in the signal-to-noise ratio, but it has also reduced the complexity of the spectrum. This allowed the range of observed A-state levels to be extended down to $v' = 6$.

The transitions obtained from the laser excitation spectrum of I_2 were used to calibrate the IBr lines in the excitation spectrum [14, 15]. In the region near 12 300 cm^{-1} where the 6–3 band is centered, only weak I_2 transitions could be observed, so the iodine cell was heated to about 140°C. Calibration of the

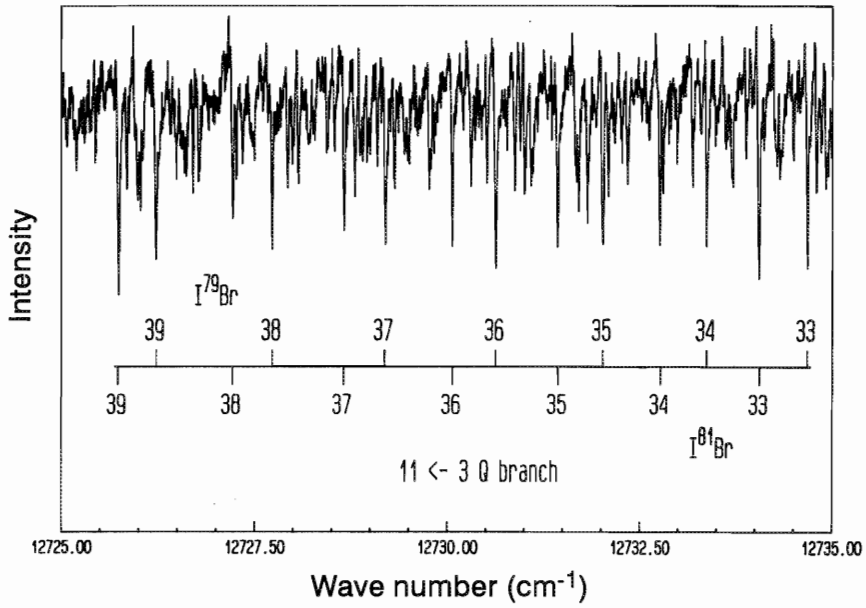

FIG. 1. Absorption spectrum showing part of the Q-branches of the 11–3 bands of the two isotopomers of IBr.

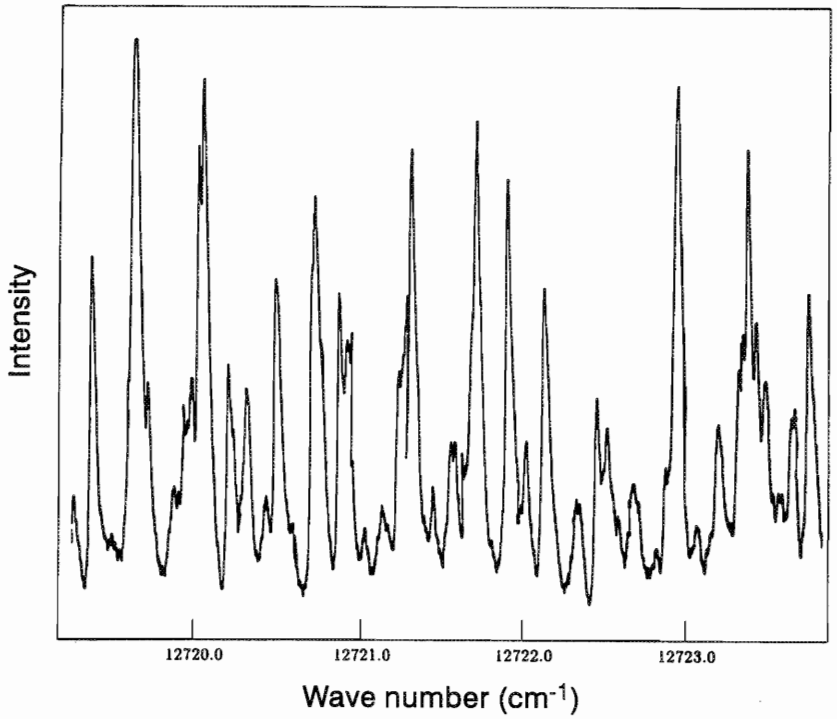

FIG. 2. Excitation spectrum showing part of the 8–2 band of $I^{79}Br$.

Fourier transform data was accomplished by using the transitions of the 9–2 band common to both experiments. The calibration factor for the Fourier transform data was calculated to be 1.000 000 564; this yielded line position shifts ranging between 0.007 and 0.008 cm^{-1}.

The absolute frequencies of the transitions observed in this study were compared with those reported by Selin [2] and Suzuki and Fujiwara [8]. While the latter are in good agreement with the present results, Selin's rovibronic data were found to be displaced from our calibrated line positions by, on average, $-0.035(\pm 0.006)$ cm^{-1}. A listing of the assigned transitions measured in the present work may be obtained by sending a request via electronic mail to :bernath @ uwaterloo.ca

3. Analysis and results

3.1. The data used in the analysis

The present analysis is based on performing direct "global" least-squares fits to four different types of data: (*i*) microwave and infrared measurements of level spacings within the $X^1\Sigma^+$ state, (*ii*) fluorescence series delineating spacing of X-state levels

TABLE 2. Characteristics of the several types of data utilized in the present analysis; $\bar{u}(Y_{obs})$ is the average uncertainty associated with each type of data

Data type	Source	No. data	X state		A-state	$\bar{u}(Y_{obs})$
			v range	J range	v range	(cm^{-1})
Visible $A-X$ absorption	Present work	7633	1–4	8–100	9–29	0.005
$A-X$ laser excitation	Present work	263	2, 3	4–42	6–9	0.003
Visible $A-X$ absorption	Ref. 8	38	2–4	9–66	7–15	0.003
Microwave	Refs. 6, 7	31	0–5	43–95	—	1×10^{-6}
Microwave	Ref. 3	6	0–2	3	—	2×10^{-7}
Infrared absorption	Footnote 2	714	0–2	5–111	—	1×10^{-4}
Visible $B'-X$ fluorescence	Refs. 4, 5	196	0–19	18–74	—	0.13
A-state B_v values	Ref. 11	4	—	—	0–2	0.000 026
A-state $T_{v,0}$ values	Ref. 11	5	—	—	0–2	0.066

up to $v = 19$, (*iii*) visible transitions defining separations between particular A- and X-state levels, and (*iv*) $T_{v,0}$ and B_v values for the three lowest levels of the $A\,^3\Pi(1)$ state. In all of these fits, the data for the two isotopomers $I\,^{79}Br$ and $I^{81}Br$ were treated simultaneously in a combined isotopes analysis. The character, range, source, and accuracy of these different types of data are summarized in Table 2. It is clear that while the visible data obtained in the present work are by far the most extensive, the other types of measurements are critical, in that they are either of higher precision or they probe regions of v' or v'' not spanned by the present results.

In global least-squares fits such as those reported below, each experimental datum Y_{obs} (i) should be weighted by the inverse square of its uncertainty u (Y_i), and the overall quality of fit characterized by the "dimensionless standard error" (or reduced χ^2)

$$\bar{\sigma} = \sqrt{\frac{\chi^2}{N_d - N_p}}$$

$$= \sqrt{\frac{\left(\sum_{i=1}^{N_d} [Y_{calc}(i) - Y_{obs}(i)]^2 / u(Y_i)^2 \right)}{(N_d - N_p)}} \qquad (1)$$

where $Y_{calc}(i)$ is the value of datum-i predicted using a model whose N_p parameters were determined from a fit to the N_d data. However, while individual uncertainties were reported for each of the microwave transitions of ref. 3 and for the v' (A) = 0 and 1 constants of ref. 11, the analogous uncertainties associated with the other types of literature data were not clear. Values for the latter were therefore determined in the following manner. After making an initial estimate of a representative average incertainty $\bar{u}(Y_{obs})$ for each type of data, fits were performed to one of the best of the models presented below, and these $\bar{u}(Y_{obs})$ values were varied until the $\bar{\sigma}$ value associated with each separate type of data became approximately unity. This yielded the $\bar{u}(Y_{obs})$ values shown in the last column of Table 2. As a final step, the individual weights were reduced for the small fraction of the data for which the discrepancies with the predictions of the model were more than four times the associated $\bar{u}(Y_{obs})$ values.

As mentioned above, for the absorption and laser excitation data obtained here the uncertainties in the positions of the best defined lines were 0.003 cm^{-1}. However, the high density of the absorption spectrum (see Fig. 2) and the widely varying intensities of different bands means that many of its lines are blended or affected by noise and, as a result, the average line position uncertainties for most bands are closer to 0.005 cm^{-1}. Because of the expected influence of perturbations, band-by-band fits were used to provide further checks on the internal consistency of these data. In particular, with the X-state constants held fixed at values determined from a fit to the microwave, infrared, and fluorescence data, the present $A-X$ data for one v' value at a time were fitted to expressions depending on the vibrational energy and inertial and centrifugal distortion constants. Lines for which the discrepancies from the model were larger than four times the average uncertainty were then given reduced weights in the subsequent global fits. The growth in the number of such lines at high v' is consistent with the expected growing importance of perturbations.

3.2. The model used in the fits

Assuming the validity of both the clamped-nuclei Born–Oppenheimer approximation and the first-order WKB approximation for the eigenvalues of a given potential energy curve, and neglecting Ω doubling and related effects, the vibration–rotation eigenvalues for all isotopomers of a diatomic molecule in a given electronic state are given by the expression [16, 17]

$$E(v, J) = \sum_{m=0}^{m^E_{max}} \sum_{l=0}^{l^E_{max}(m)} \bar{Y}_{l,m} \frac{\left(v + \frac{1}{2}\right)^l [\kappa^2]^m}{\mu^{(m+l/2)}} \qquad (2)$$

where $\kappa^2 = J(J+1) - \Omega^2$, v and J are the usual vibrational and rotation quantum numbers, Ω the projection of the total electronic angular momentum on the diatom axis, μ the molecular reduced mass, and the coefficient $\bar{Y}_{0,0} = 0$. The breakdown of these two approximations may be accounted for by allowing $\bar{Y}_{0,0}$ to be non-zero and by multiplying each term in (2) by a factor $\left\{1 + \frac{m_e}{M_A}\Delta^A_{l,m} + \frac{m_e}{M_B}\Delta^B_{l,m}\right\}$, where m_e is the electron mass, M_A and M_B the masses of atoms A and B, and $\Delta^A_{l,m}$ and $\Delta^B_{l,m}$ are mass-independent constants [18–21]. For molecules formed from heavy atoms, these correction terms are usually so small that they are difficult to determine in empirical analyses.

Since our experimental data set contains results for two isotopes of bromine but only one isotope of iodine (^{127}I), an empirical analysis would at best only be able to determine values

for $\Delta^{Br}_{l,m}$, with any effects due to $\Delta^{I}_{l,m}$ being incorporated into the $\bar{Y}_{l,m}$ values. Campbell and Bernath [10] concluded that for the ground electronic state of IBr it was possible to determine the correction factor $\Delta^{Br}_{1,0}$.[3] In the present analysis, the energies of $X^1\Sigma^+$-state levels were therefore represented by the expression

$$E_X(v,J) = \sum_{m=0}^{m^E_{max}} \sum_{l=0}^{l^E_{max}(m)} \bar{Y}_{l,m} \left\{1 + \frac{m_e}{M_{Br}} \Delta^{Br}_{l,m}\right\} \times \frac{\left(v+\frac{1}{2}\right)^l [J(J+1)]^m}{\mu^{(m+l/2)}} \quad (3)$$

with trial and error tests (see below) being used to determine how many terms to include in the expansions over m and l, and which values of $\Delta^{Br}_{l,m}$ may be determined reliably.

The relatively high resolution of the microwave and infrared data available for the ground $X^1\Sigma^+$ state of IBr (see Table 2) raises the possibility of determining $\Delta^{Br}_{l,m}$ value(s) for that state, in spite of the relatively large atomic masses. However, the fact that the visible absorption data are of somewhat lower resolution and do not extend below $v' = 6$, together with the even larger uncertainties and indirect nature of the information on its lowest three levels, precludes the determination of such correction terms for the $A^3\Pi(1)$ state. On the other hand, requiring internal consistency between the data for the two isotopomers does make it possible to determine the effective displacement between their A-state electronic energies:

$$\Delta T_e^{eff}(A) = {}^{81}T_e^{eff}(A) - {}^{79}T_e^{eff}(A) \quad (4)$$

where ${}^iT_e^{eff}(A)$ is the effective electronic energy for the A state of the isotopomer involving ^{i}Br. These are "effective" electronic energies, since they subsume both Born–Oppenheimer breakdown effects, due to the fact that the potential energy curves for the two isotopomers are not exactly the same, and the effects of higher order WKB terms that give rise to non-zero $\bar{Y}_{0,0}$ values. For simplicity, the values of ${}^iT_e^{eff}(A)$ reported below assume a zero of energy based on neglect of the zero-point energy corrections $\bar{Y}_{0,0}$ for both electronic states.

Since the A state has electronic quantum number $\Omega = 1$, its rotational levels are subject to Ω doubling, which splits each one into e and f components by addition of the energy $\pm\{(q_v^B/2)[J(J+1)-1]+\ldots\}$, where the + sign is associated with the e-parity levels and the − sign with the f ones. If the Ω-doubling constants are expanded in terms of a power series in $\left(v+\frac{1}{2}\right)$,

$$\frac{q_v^B}{2} = \sum_{l=0}^{l^q_{max}(1)} Q_{l,1}\left(v+\frac{1}{2}\right)^l \quad (5)$$

the energies of A-state vibration–rotation levels may be written as

[3] Note that a typographical error in ref. 10 led to this coefficient being incorrectly identified there as $\Delta^{Br}_{0,1}$.

TABLE 3. Numbers of A-state expansion parameters and dimensionless standard error $\bar{\sigma}$ of the best fit for various choices of v'_{max}

v'_{max}	$n_{G'}$	$n_{B'}$	$n_{D'}$	$n_{Q_B'}$	$\bar{\sigma}$
16	6	5	3	2	1.39
17	6	6	3	2	1.39
18	7	7	3	2	1.40
19	7	7	3	2	1.43
20	8	7	3	2	1.43
21	9	8	3	2	1.50
22	9	8	3	2	1.54
23	10	8	4	2	1.54
24	10	8	4	2	1.56
25	10	8	5	2	1.77
26	11	8	5	2	1.82
27	12	8	7	2	3.01
28	12	8	9	2	7.62
29	12	9	9	2	10.88

$$E_A(v,J) = {}^iT_e^{eff} + \sum_{m=0}^{m^E_{max}} \sum_{l=0}^{l^q_{max}(m)} (\bar{Y}_{l,m} \pm \bar{Q}_{l,m}) \times \frac{\left(v+\frac{1}{2}\right)^l [J(J+1)-1]^m}{\mu^{(m+l/2)}} \quad (6)$$

where $Q_{l,m} = \bar{Q}_{l,m}/\mu^{(m+l/2)}$, all $\bar{Q}_{l,m}$ coefficients are identically zero for $m = 0$, and (again) the + and − signs are associated with the e- and f-parity levels, respectively. This is the expression used to represent the A-state energies in the present fits.

In utilizing the results of Clevenger et al. [11] in the present analysis, the A-state B_v values and energies were represented by the usual Dunham expansions involving the same coefficients appearing in (6):

$$B_v = \sum_{l=0}^{l^E_{max}(1)} \bar{Y}_{l,1} \frac{\left(v+\frac{1}{2}\right)^l}{\mu^{(1+l/2)}} \quad (7)$$

$$T_{v,0} = {}^iT_e^{eff} = \sum_{l=1}^{l^E_{max}(0)} \bar{Y}_{l,0} \frac{\left(v+\frac{1}{2}\right)^l}{\mu^{l/2}} - \text{Z.P.E.}(X) \quad (8)$$

where Z.P.E.(X) is the vibrational zero point energy for the X state calculated from the Dunham coefficients associated with (3).

In conclusion, therefore, the present analysis involves performing simultaneous least-squares fits of the several types of data listed in Table 2 to energy differences and the A-state energies and B_v values defined by (3) and (6)–(8). In addition, the upper state energy $E_{B'}$ (v' J') of each of the eight B'–X flourescence series observed by Weinstock and Preston [4, 5] was treated as a free parameter in the fits. Together with these $E_{B'}$ (v' J') values, the parameters determined from these fits are the usual sets of $\bar{Y}_{l,m}$ coefficients for the X and A states, the effective A-state electronic energies ${}^iT_e^{eff}$ for the two isotopomers, and any determinable $\Delta^{Br}_{l,m}$ constants for the X state and $\bar{Q}_{l,m}$ constants for the A state. Choosing to represent the products $(\bar{Y}_{l,m}\Delta^{Br}_{l,m})$ in (3) by the composite parameters $\delta^{Br}_{l,m}$ makes these fits remain linear, while the correct

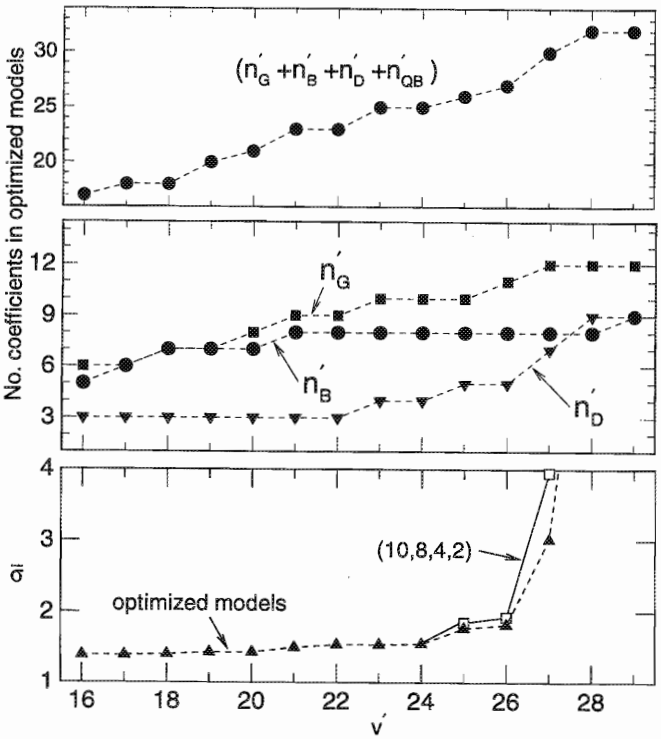

FIG. 3. Dependence on v'_{max} of the dimensionless standard deviation $\bar{\sigma}$ (lowest segment) and of the numbers of A-state parameters (upper segments) required by the optimum Dunham model for the fit.

uncertainties in the $\Delta^{Br}_{l,m}$ parameters may readily be generated from the uncertainties in the fitted $\bar{Y}_{l,m}$ and $\delta^{Br}_{l,m}$ values and the appropriate elements of the correlation matrix. It also turns out that the difference ΔT_e^{eff} may be determined with much greater accuracy than the individual $^{i}T_e^{eff}$ values, so by using (4) to define $^{81}T_e^{eff}$ the electronic energy parameters actually varied in the fits were $^{79}T_e^{eff}$ and ΔT_e^{eff}.

3.3. Determining the optimum model and molecular constants

To determine the optimum representation of the data for the $A-X$ system of IBr, it is necessary to ascertain how many terms should be included in each of the vibrational and rotational expansions. In other words, it is necessary to determine optimum sets of values of $l^E_{max}(m)$ for the X- and A-state sums of (3) and (6), values of $l^q_{max}(m)$ for the A state, and which (if any) correction coefficients $\Delta^{Br}_{l,m}$ may be determined from these data. The quality of fit and its dependence on the numbers of parameters included in the model are the main criteria used for identifying the optimum model.

Experimentation with a wide range of models showed that, for the X state, the rotational sum of (3) may be truncated at $m^E_{max} = 3$. For the A state, the fits require only $m^E_{max} = 2$ in (6), and they also require only an $m^q_{max} = 1$ expansion to define the Ω-doubling energies characterized by the $\bar{Q}_{l,1}$ constants. In other words, no centrifugal distortion Ω-doubling parameters were required to account for the existing data.

With regard to the X-state $\Delta^{Br}_{l,m}$ parameters, fits to the microwave and infrared data, with or without inclusion of the $B'-X$ fluorescence emission data, showed that inclusion of such terms for $(l, m) = (1, 0)$ and (or) $(0, 1)$ improved the quality of fit by less than 0.3%, while the resulting constants had 95% confidence limit uncertainties greater than 100% of their values. Moreover, the signs of those constants were the opposite

TABLE 4. Present recommended Dunham constants for the X state of IBr (in cm^{-1}), and their 95% confidence limit uncertainties

	$I^{79}Br$	$I^{81}Br$	Uncertainty
$Y_{1,0}$	268.681 42	266.628 35	1.1×10^{-4}
$Y_{2,0}$	$-0.816\,913$	$-0.804\,477$	7.2×10^{-5}
$Y_{3,0}$	-1.3060×10^{-3}	-1.2762×10^{-3}	1.5×10^{-5}
$Y_{4,0}$	-1.24×10^{-5}	-1.21×10^{-5}	6.8×10^{-7}
$Y_{0,1}$	0.056 832 589	0.055 967 362	2.1×10^{-8}
$Y_{1,1}$	$-1.969\,58 \times 10^{-4}$	$-1.924\,77 \times 10^{-4}$	2.2×10^{-8}
$Y_{2,1}$	-4.469×10^{-7}	-4.334×10^{-7}	1.0×10^{-8}
$Y_{3,1}$	-6.1×10^{-9}	-5.9×10^{-9}	1.6×10^{-9}
$Y_{0,2}$	$-1.016\,71 \times 10^{-8}$	$-0.985\,99 \times 10^{-8}$	3.1×10^{-12}
$Y_{1,2}$	-4.99×10^{-11}	-4.80×10^{-11}	1.0×10^{-12}
$Y_{0,3}$	-1.60×10^{-15}	-1.53×10^{-15}	1.9×10^{-16}

of those reported by Campbell and Bernath [10] and by Clevenger et al. [11]. Since the microwave data were the same while the infrared data used in the present analysis (see footnote 2) are more extensive and more accurate than those used in refs. 10 and 11, we conclude that it is not possible to determine statistically significant values of *any* $\Delta^{Br}_{l,m}$ parameters from the existing data for this system, and that the values reported in refs. 10 and 11 are likely not reliable.

Models based on a wide range of sets of $\{l^E_{max}(m)\}$ values were considered, with each fit being identified by the number of terms included in the vibrational expansion (over l) for each value of m. The integers $n_G = l^E_{max}(m = 0)$, $n_B = l^E_{max}(1) + 1$, $n_D = l^E_{max}(2) + 1$ and $n_H = l^E_{max}(3)+1$ indicate the numbers of terms included in the various expansions of (3) and (6), while $n_{Q_B} = l^q_{max}(1) + 1$ defines the number of terms retained in the expansion of (5). (As usual, the $m = 0$ sums begin at $l = 1$, while all the others start from $l = 0$.) Thus, a particular model for the X state may be labelled by the set of integers $(n''_G, n''_B, n''_D, n''_H)$, while one for the A state is identified by $(n'_G, n'_B, n'_D, n'_{Q_B})$.

Although Selin only explicitly identified A-state levels above $v' = 29$ as being perturbed [2], the fact that the molecular constants he reported were based on only data for $v' \leq 16$ leaves open the possibility that perturbations may also affect levels in the intermediate region. To examine this question, sets of fits were were performed that took account of all of the available information on the X state, but excluded data involving A-state vibrational levels lying above a selected cutoff of $v' = v'_{max}$. As v'_{max} is increased from 16 to 29, the behaviour of $\bar{\sigma}$ for the best model for each case should delineate the onset of significant perturbations.

For $v'_{max} = 16$, a case for which no A-state perturbations are expected to arise, fits to a range of possible models showed that an optimum representation of this data set was obtained with an X-state model defined by $(n''_G, n''_B, n''_D, n''_H) = (4, 4, 2, 1)$, where the associated model for the A state was that defined by the integers listed in the first row of Table 3. Since the data accessing the higher A-state levels do not involve a broader range of X-state levels, this X-state model was used in all subsequent fits, although the constants themselves were allowed to vary freely in each case.

For values of v'_{max} ranging from 16 to 29, fits were performed to a range of $(n'_G, n'_B, n'_D, n'_{Q_B})$ models, and an optimum model selected from consideration of the value of $\bar{\sigma}$ and of the uncertainties in the leading fitted parameters. For each v'_{max}, the integers defining the resulting "best" A-state model are listed in Table 3, together with the associated values of $\bar{\sigma}$. The dependence of these optimum $\bar{\sigma}$ values on v'_{max} is shown by the solid points

TABLE 5. Present recommended Dunham constants for the A state of IBr (in cm^{-1}), and their 95% confidence limit uncertainties

	$I^{79}Br$	$I^{81}Br$	Uncertainty
$^{79}T_e$ (eff)	12 370.010 7	—	3.6×10^{-2}
ΔT_e (eff)	—	−0.006 3	3.8×10^{-4}
$Y_{1,0}$	133.450 61	132.430 88	8.9×10^{-2}
$Y_{2,0}$	−0.608 972 5	−0.599 701 4	5.9×10^{-2}
$Y_{3,0}$	−0.335 302 81	−0.327 674 98	1.9×10^{-2}
$Y_{4,0}$	0.062 778 360	0.060 881 417	3.6×10^{-3}
$Y_{5,0}$	$-7.751\,786\,31 \times 10^{-3}$	$-7.460\,110\,83 \times 10^{-3}$	4.2×10^{-4}
$Y_{6,0}$	$6.144\,535\,93 \times 10^{-4}$	$5.868\,150\,90 \times 10^{-4}$	3.1×10^{-5}
$Y_{7,0}$	$-3.141\,858\,22 \times 10^{-5}$	$-2.977\,607\,61 \times 10^{-5}$	1.5×10^{-6}
$Y_{8,0}$	$9.973\,765\,87 \times 10^{-7}$	$9.380\,127\,65 \times 10^{-7}$	4.7×10^{-8}
$Y_{9,0}$	$-1.774\,571\,05 \times 10^{-8}$	$-1.656\,195\,76 \times 10^{-8}$	8.1×10^{-10}
$Y_{10,0}$	$1.346\,397\,75 \times 10^{-10}$	$1.246\,982\,48 \times 10^{-10}$	6.1×10^{-12}
$Y_{0,1}$	0.042 426 33	0.041 780 43	4.6×10^{-5}
$Y_{1,1}$	$-6.396\,15 \times 10^{-4}$	$-6.250\,64 \times 10^{-4}$	3.2×10^{-5}
$Y_{2,1}$	$1.027\,750 \times 10^{-4}$	$0.996\,695 \times 10^{-4}$	9.7×10^{-6}
$Y_{3,1}$	$-1.995\,025 \times 10^{-5}$	$-1.919\,958 \times 10^{-5}$	1.4×10^{-6}
$Y_{4,1}$	$1.941\,4384 \times 10^{-6}$	$1.854\,1113 \times 10^{-6}$	1.2×10^{-7}
$Y_{5,1}$	$-1.066\,5272 \times 10^{-7}$	$-1.010\,7711 \times 10^{-7}$	5.6×10^{-9}
$Y_{6,1}$	$3.007\,491 \times 10^{-9}$	$2.828\,485 \times 10^{-9}$	1.3×10^{-10}
$Y_{7,1}$	$-3.349\,161 \times 10^{-11}$	$-3.125\,751 \times 10^{-11}$	1.3×10^{-12}
$Y_{0,2}$	-5.120×10^{-8}	-4.965×10^{-8}	3.7×10^{-9}
$Y_{1,2}$	7.981×10^{-9}	7.681×10^{-9}	7.4×10^{-10}
$Y_{2,2}$	$-7.184\,2 \times 10^{-10}$	-6.8610×10^{-10}	4.8×10^{-11}
$Y_{3,2}$	$1.185\,4 \times 10^{-11}$	1.1234×10^{-11}	1.0×10^{-12}
$Q_{0,1}$	-1.83×10^{-6}	-1.80×10^{-6}	3.0×10^{-7}
$Q_{1,1}$	4.99×10^{-7}	4.87×10^{-7}	1.9×10^{-8}

TABLE 6. Energies determined for the B'-state level initial states of the fluorescence series observed by Weinstock and Preston [4, 5], expressed relative to the ground state potential minimum, and their 95% confidence limit uncertainties

$I^{79}Br$		$I^{81}Br$	
(v', J')	$E_{B'}(v' J')$ (cm^{-1})	(v', J')	$E_{B'}(v' J')$ (cm^{-1})
(20, 33)	18 036.396 (±0.016)	(11, 19)	17 538.515 (±0.017)
(20, 34)	18 038.257 (±0.013)	(11, 21)	17 541.050 (±0.015)
(21, 58)	18 142.330 (±0.018)	(15, 41)	17 803.015 (±0.017)
(22, 73)	18 233.806 (±0.011)	(20, 45)	18 054.312 (±0.013)

joined by broken lines in the bottom segment of Fig. 3. The two upper segments of this figure then show how the total number of fitted parameters and the numbers of parameters in the individual $m(A) = 0$, 1 and 2 expansions vary with v'_{max}. Another view of the effect of increasing the range of A-state levels considered is obtained if the same model is used in fits for a range of v'_{max} values. To this end, the square open points joined by solid lines in the bottom segment of Fig. 3 show the behaviour of $\bar{\sigma}$ for the model determined as "best" for the data sets associated with $v'_{max} = 16$ and 24, respectively.

The plots in the lowest segment of Fig. 3 show that $\bar{\sigma}$ begins to grow distinctly more rapidly above $v'_{max} = 24$, and we found that no increases in the numbers of A-state expansion parameters changed this situation. This is taken as evidence that the vibration–rotation data involving A-state levels above $v' = 24$ are increasingly perturbed, in that they cannot be explained by the simple Dunham model underlying (6). Therefore, the $(n''_G, n''_B, n''_D, n''_H) = (4, 4, 2, 1)$ and $(n'_G, n'_B, n'_D, n'_{Q_B}) = (10, 8, 4, 2)$ model for $v'_{max} = 24$ is taken as providing the best set of unperturbed molecular constants for the A–X system. The resulting recommended spectroscopic constants are listed in Tables 4–6; the large numbers of significant figures in the reported parameters ensure that all of the observed transition frequencies used in the fits could be reproduced to within at least 10% of their uncertainties. Note that while the Dunham constants actually listed in Tables 4 and 5 are the value ${}^iY_{lm} = Y_{lm}/\mu_i^{(m+l/2)}$ and ${}^iQ_{l1}/\mu_i^{(1+l/2)}$ for the individual isotopomers, the fits actually determine the single set of mass-reduced parameters $\{Y_{lm}\}$ and $\{Q_{l1}\}$.

Although the recommended A-state molecular constants of Table 5 are only valid for levels up to $v' = 24$, the new absorption data extend to $v' = 29$. While these last five levels are believed to suffer from significant perturbations, it seems useful to present preliminary results for them. To this end, Table 7 lists term energies and rotational and centrifugal distortion constants for these levels obtained from fits to our data for one v' level at a time with the ground state constants held fixed at the optimized values given in Table 4.

4. Concluding remarks

Extensive new high-resolution visible absorption and laser excitation measurements have been combined with appropriately weighted earlier microwave, infrared, and visible fluorescence data, as well as with energies and B_v values for the three lowest levels of the A state, and used in direct fits to mass-reduced Dunham expansions to yield new spectroscopic constants for the $A^3\Pi(1)$ and $X^1\Sigma^+$ states of IBr. While Selin had noted that A- state vibrational levels lying above $v' = 29$ were perturbed, the present analysis indicates that perturbations begin to become significant above $v' = 24$. Thus, although the data set actually extends to A-state level $v' = 29$, the present recommended molecular constants were based on transitions involving $v' \leq 24$; however, this still spans approximately 85%

TABLE 7. Energies (relative to the X-state potential minimum) and rotational constants for A-state levels lying above the range represented by the recommended constants of Table 5 (all in cm^{-1}). The 95% confidence limit uncertainties, in terms of the final digits shown, are given in parentheses

Species	v	$E_A(v)$	B_v	$D_v/10^{-7}$	$(q_v^B/2)/10^{-5}$
$I^{79}Br$	25	14 507.092 (4)	0.025 168 (8)	0.85 (3)	2.4 (2)
	27	14 565.813 (4)	0.023 616 (5)	1.92 (1)	1.4 (1)
	28	14 591.942 (3)	0.022 814 (4)	3.96 (1)	5.3 (1)
	29	14 615.893 (5)	0.021 938 (12)	4.85 (5)	3.0 (2)
$I^{81}Br$	25	14 500.839 (4)	0.024 993 (6)	1.11 (2)	1.2 (2)
	26	14 531.633 (8)	0.024 155 (13)	1.11 (4)	1.4 (1)
	27	14 560.103 (3)	0.023 365 (4)	1.32 (1)	1.2 (1)
	28	14 586.465 (4)	0.022 542 (7)	1.53 (3)	1.5 (1)
	29	14 610.849 (7)	0.021 703 (4)	1.90 (6)	0.7 (2)

of the A-state well depth. In contrast, the range of levels $v'' = 0-19$ spanned by our recommended X-state constants is approximately one third of the ground state well depth.

It was pointed out above that the effective A-state electronic isotope shift $\Delta T_e^{eff} = -0.0063\ (\pm 0.0004)\ cm^{-1}$ determined here includes effects due to both Born–Oppenheimer breakdown and neglect of the higher-order WKB corrections giving rise to the zero-point energy corrections, ${}^iY_{0,0}$. Since values of ${}^iY_{0,0}$ for the two isotopomers may be calculated from a knowledge of their other $Y_{l,m}$ constants [22], it is possible in principle to determine the Born–Oppenheimer breakdown electronic energy shift $\Delta T_e^{BO}(A)$ from the difference

$$\begin{aligned}\Delta T_e^{BO}(A) &= \Delta T_e^{eff}(A) - \Delta T_e^{WKB}(A) \\ &= \Delta T_e^{eff}(A) - \{[{}^{81}Y_{0,0}^{A} - {}^{81}Y_{0,0}^{X}] \\ &\quad - [{}^{79}Y_{0,0}^{A} - {}^{79}Y_{0,0}^{X}]\} \qquad (9)\end{aligned}$$

However, the uncertainties in the calculated values of $\Delta T_e^{WKB}(A)$ are much larger than $\Delta T_e^{eff}(A)$, so is impossible to distinguish between these two types of effects in the present analysis.

There exist substantial differences between the A-state spectroscopic constants obtained here and those reported by Selin [2] and by Suzuki and Fujiwara [8]. Although the present absorption and laser excitation data are more accurate and comprehensive than those used in their analyses, the largest differences are due to our utilization of the Clevenger et al. [11] data, which provide the first direct information on the lowest vibrational levels of the A state. At the same time, transitions observed in the present absorption and laser excitation experiments were found to be in good agreement with those reported by Suzuki and Fujiwara [8], but disagreed with Selin's data by an average shift of $-0.035\ cm^{-1}$.

In very recent work, Clevenger et al. [11] reported an analysis that was quite similar to that presented here, in that it combined their deperturbed constants for A-state levels $v = 0-2$ with extensive visible absorption measurements, with the $B'-X$ fluorescence data of Weinstock and Preston [4, 5], and with microwave and infrared data for the ground state. However, the infrared data they used was that of Campbell and Bernath [10], which is somewhat less accurate and spans one fewer vibrational level than the very recent results of Nelander et al. (see footnote 2) used here, while for the visible region they had to rely on the data of Selin [2], which is less accurate and does not reach as low v' values as the new Fourier transform results reported herein. Their analysis did explicitly require that the X- and A-state centrifugal distortion constants be "mechanically consistent" with the potential implied by the vibrational energies and B_v values. However, although such constraints were not imposed in the present empirical analysis, the present fitted $Y_{0,2}$, $Y_{1,2}$, and $Y_{0,3}$ constants for the X state are within 0.4, 5.6, and 17% of the values implied by the lower order constants [22]. For the A state, the analogous discrepancies for $Y_{0,2}$, and $Y_{1,2}$ are very much larger; however, in the absence of any high-J data for the lowest vibrational levels, these discrepancies have little significance.

Acknowledgements

We are very grateful to Professor J. Tellinghuisen for providing us with a preprint of ref. 11, and we are pleased to acknowledge helpful discussions with Dr. M. Dulick.

1. W.G. Brown. Phys. Rev. **42**, 335 (1932).
2. L.E. Selin. Ark. Fys. **27**, 479 (1962).
3. E. Tiemann and Th. Möller. Z. Naturforsch. **30A**, 986 (1975).
4. E.M. Weinstock. J. Mol. Spectrosc. **61**, 395 (1976).
5. E.M. Weinstock and A. Preston. J. Mol. Spectrosc. **70**, 188 (1978).
6. R.E. Willis. Ph.D. Thesis, Department of Physics, Duke University. 1979.
7. R.E. Willis and W.W. Clark III. J. Chem. Phys. **72**, 4946 (1980).
8. M. Suzuki and T. Fujiwara. J. Mol. Spectrosc. **133**, 233 (1989).
9. X. Zheng, M.C. Heaven, and J. Tellinghuisen. Chem. Phys. Lett. **195**, 273 (1992).
10. J. Campbell and P.F. Bernath. J. Mol. Spectrosc. **158**, 339 (1993).
11. J.O. Clevenger, Q.P. Ray, J. Tellinghuisen, M.C. Heaven, and X. Zheng. Can J. Phys. **72**, 1294 (1994).
12. M. Dulick, P.F. Bernath, and R.W. Field. Can. J. Phys. **58**, 703 (1980).
13. J.C.D. Brand, O.R. Dhatt, A.R. Hoy, and D.C.P. Tse. J. Mol. Spectrosc. **119**, 398 (1986).
14. S. Gerstenkorn and P. Luc. Atlas du spectre d'absorption de la molecule d'iode. Laboratoire Aime Cotton, CNRS II, 91405 Orsay, France. 1977.
15. S. Gerstenkorn and P. Luc. Rev. Phys. Appl. **14**, 791 (1979).
16. J.L. Dunham. Phys. Rev. **41**, 713 (1932).
17. J.L. Dunham. Phys. Rev. **41**, 721 (1932).
18. A.H.M. Ross, R.S. Eng, and H. Kildal. Opt. Commun. **12**, 433 (1974).
19. J.K.G. Watson. J. Mol. Spectrosc. **45**, 99 (1973).
20. J.K.G. Watson. J. Mol. Spectrosc. **80**, 411 (1980).
21. P.R. Bunker. J. Mol. Spectrosc. **68**, 367 (1977).
22. G. Herzberg. Spectra of diatomic molecules. Van Nostrand, Toronto. 1950.